

Article

Preparation of a Master Fe–Cu Alloy by Smelting of a Cu-Bearing Direct Reduction Iron Powder

Liaoting Pan, Deqing Zhu, Zhengqi Guo * and Jian Pan

School of Mineral Processing and Bioengineering, Central South University, Changsha 410083, China; plt6299@126.com (L.P.); dqzhu@csu.edu.cn (D.Z.); pjcsu@csu.edu.cn (J.P.)

* Correspondence: guozqcsu@csu.edu.cn; Tel.: +86-185-7313-1417; Fax: +86-731-8883-6942

Received: 13 May 2019; Accepted: 18 June 2019; Published: 21 June 2019



Abstract: Generally, the Cu-bearing direct reduction iron powder (CBDRI) obtained from a direct reduction-magnetic separation process of waste copper slag contains a high content of impurities and cannot be directly used to produce Cu-bearing special steel. In this paper, further smelting treatment of CBDRI was conducted to remove its impurities (such as S, SiO₂, Al₂O₃, CaO and MgO) and acquire a high-quality Fe–Cu master alloy. The results show that the Fe–Cu master alloy, assaying 95.9% Fe, 1.4% Cu and minor impurities, can be obtained from the smelting process at 1550 °C for 40 min with 1.0 basicity. Meanwhile, the corresponding iron and copper recoveries are 98.6% and 97.2%, respectively. Theoretical calculations and experimental results show that appropriate basicity (0.9~1.1) is beneficial for the recovery of Fe and Cu from a thermodynamic viewpoint due to the excellent fluidity of the slag in this basicity range. Moreover, the mechanism of desulfurization was revealed by calculating the sulfide capacity and the desulfurization reaction kinetics. Increasing the binary basicity of the slag benefits both the sulfide capacity and diffusion coefficient of the sulfur in the molten slag, resulting in higher desulfurization efficiency and lower S content in the master alloy.

Keywords: Cu-bearing direct reduction iron; smelting; Cu-bearing steel; basicity; sulfide capacity; desulfurization

1. Introduction

Cu-bearing steel is characterized by high strength, excellent corrosion resistance and high antibacterial ability [1–4]. Based on this characterization, many kinds of Cu-bearing steels, such as weathering steel, antibacterial stainless steel and high-strength steel (HSAL serials), have been rapidly developed in recent years [5–7]. Generally, conventional Cu-bearing steel production methods require the addition of electrolytic copper to adjust the copper content in the products [8–10]. Unfortunately, with the depletion of high-grade copper mineral resources in the world, the production costs for electrolytic copper remains high. This problem could ultimately lead to higher production costs for Cu-bearing steel. However, low-cost ferroalloy (Fe–Cu alloy) may replace electrolytic copper in the production of the Cu-bearing steels, which provides the possibility of innovation lowering technology costs.

Copper smelting slag typically contains 40% Fe and 1% Cu and can be considered as an important secondary resource for utilization [11]. Recently, researchers have proposed processes to recover valuable metals from copper slag [12–17]. However, those processes mainly focused on Cu recovery while totally neglecting Fe recovery. Direct reduction process, as a novel process, was developed to treat the copper slag [8,10,18–22]. In this process, the iron oxides and copper bearing minerals were reduced to metallic iron and copper. The metallic copper dissolves into metallic Fe lattices to form a Fe–Cu solid solution (Fe–Cu alloy). The Fe–Cu solid solution can then undergo subsequent grinding and magnetic separation processes. Therefore, this process can fulfil the comprehensive recovery of Fe and Cu from copper slag and attain Fe–Cu direct reduction iron powder (CBDRI). CBDRI could

potentially substitute for scrap steel and electrolytic copper in the production of Cu-bearing steel and may lead to lower costs for steel production. However, most CBDRI is not suitable for being directly used in steel production due to its high impurity concentration (SiO_2 , Al_2O_3 , CaO , MgO and S), therefore, a necessary extra smelting step to remove those impurities and obtain a higher Fe–Cu alloy purity is indispensable. There are few investigations, however, on CBDRI for the production of Cu-bearing steel master alloy via electric furnace smelting.

CBDRI has been successfully prepared from copper smelting slag by a direct reduction-magnetic separation process as reported in our earlier paper [10]. The aim of this research is to produce a high-quality Fe–Cu master alloy from CBDRI by a smelting process and directly use the master alloy as the raw material to produce Cu-bearing steel by an electric arc furnace to replace part of the electrolytic copper and scrap steel. Additionally, the desulfurization behavior and its mechanism in the smelting process were revealed in this work.

2. Experimental

2.1. Raw Materials

The Fe–Cu direct reduction iron powder (CBDRI) used in this study was obtained from the direct reduction and magnetic separation of copper smelting slag. The chemical mass composition of CBDRI shown in Table 1 and demonstrate that CBDRI contains 90.33% Fe and 1.29% Cu, which are potential materials for the preparation of copper bearing steel. Some undesirable impurities, such as SiO_2 , Al_2O_3 , CaO , and MgO , are also found in the CBDRI. In particular, the S content in CBDRI is as high as 0.3%, which is extremely harmful to the production of Cu-bearing steel. The smelting treatment of the CBDRI is necessary to ensure the quality of the alloy. Furthermore, the size distribution of CBDRI presented in Figure 1 shows that the CBDRI is very fine, with over 90% below 0.074 mm.

Table 1. Chemical compositions of CBDRI (wt %).

Fe	Cu	S	MFe	SiO_2	Al_2O_3	CaO	MgO	Na_2O	C	P
90.33	1.29	0.30	87.54	3.62	0.56	1.09	0.29	0.07	0.78	0.012

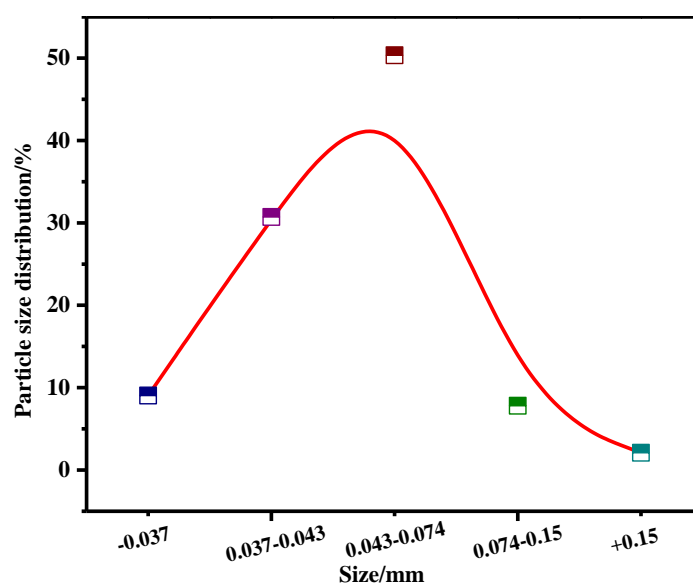


Figure 1. Size distribution of CBDRI.

The chemical composition of limestone is shown in Table 2. Limestone containing 55.73% of CaO was used as both a flux and desulfurizer to adjust the binary basicity (ratio of CaO/SiO_2) and remove sulfur in the smelting process. Its particle size was less than 0.074 mm.

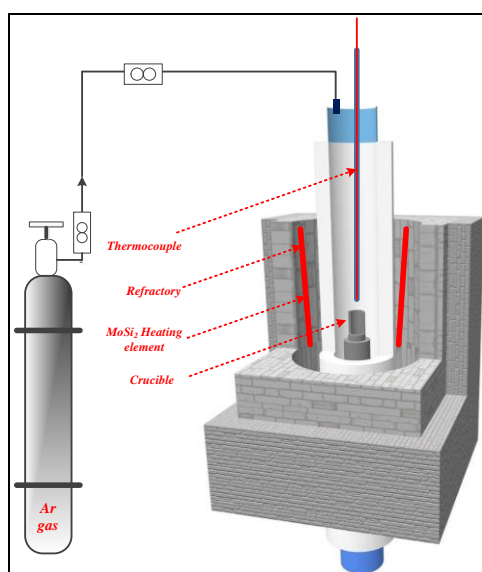
Table 2. Chemical compositions of limestone(wt %).

CaO	Al ₂ O ₃	SiO ₂	MgO	P	S	MnO	LOI
55.73	1.19	4.13	2.05	0.001	0.001	0.02	41.52

2.2. Experimental Methods

2.2.1. Smelting Process

The smelting tests were performed under a controlled environment in a vertical MoSi₂ heating furnace (schematic diagram of the smelting furnace is shown in Figure 2). The proportion integral differential (PID) temperature control programme in the furnace was used to limit the temperature fluctuation range to ± 5 °C. In each test, 30 g of CBDRI were mixed uniformly with the required amount of limestone. The mixtures were then loaded into a 50 mL corundum crucible. When the furnace temperature was raised to the smelting temperature (1515~1600 °C), the crucible was quickly placed into the heating zone of the furnace and smelted for a given period of time (10~60min) under a N₂ atmosphere. At the end of smelting, the crucible was taken out of the furnace and quickly cooled under the cover via coke breeze. Finally, the crucible was broken to separate and weigh the Fe–Cu alloy and slag carefully for sample preparation. The samples were then prepared to assay the chemical compositions.

**Figure 2.** Schematic diagram of the smelting furnace.

The recovery rate of iron and Cu η was calculated from Equation (1):

$$\eta = \frac{M_1 \times TM_1}{M_0 \times TM_0} \times 100\% \quad (1)$$

where η is the recovery rate of Fe or Cu; M_1 is the mass of the Fe–Cu master alloy; TM_1 is the grade of Fe or Cu in the master alloy; M_0 is the mass of CBDRI; TM_0 is the grade of Fe or Cu in CBDRI.

2.2.2. Analytic Tests

A thermodynamic package FactSage (Version 7.0) software (GTT-Technologies, Herzogenrath, Germany) was used to calculate the phase diagram of Fe–Cu–C, SiO₂–Al₂O₃–CaO–MgO and the viscosity of the molten slag. The phase compositions of the samples were investigated using an X-ray diffractometer (XRD, D/max 2550 PC, Rigaku Co., Ltd, Tokyo, Japan). Microstructure analyses of

master alloy were observed by a Leica DMLP optical microscopy, FEI Quanta-200 scanning electron microscope (SEM, TESCAN, MIRA3 LMU, Brno, Czech Republic) and an EDAX energy dispersive X-ray spectrometer (EDS). The SEM images were recorded in backscatter electron modes operating in the low vacuum mode at 0.5 Torr and 20 keV.

3. Results and Discussion

3.1. Thermodynamics Calculations of Smelting Process

The thermodynamics calculations for the molten slag and alloy in smelting process were conducted by FactSage 7.0 to analyse the feasibility for separation between the slag and master alloy. The quaternary phase diagram of the CaO–MgO–SiO₂–Al₂O₃ primary slag is presented in Figure 3 and shows that the primary slag possesses the appropriate liquidus temperature at approximately 1450 °C.

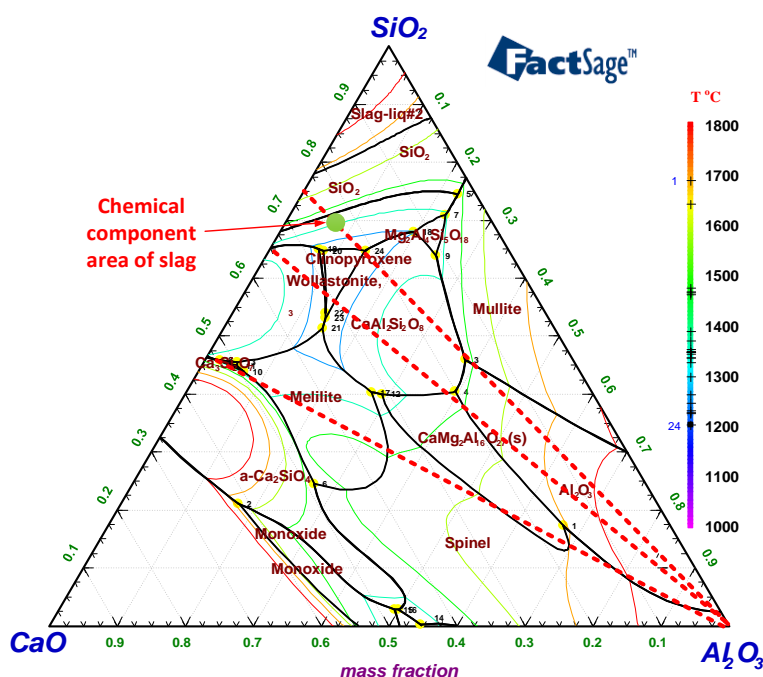


Figure 3. Phase diagram of SiO₂-Al₂O₃-CaO with MgO = 5.22%.

In addition, the liquid projection of the ternary alloy was carried out; the results are shown in Figure 4. The liquidus temperature of this ternary alloy was near 1450 °C. Based on the Figures 3 and 4, the smelting temperature should be 1500~1550 °C to ensure a good separation between alloy and slag and to keep a superheated temperature range.

3.2. Smelting Process of CBDRI

As shown in Table 1, iron and copper, as the main valuable metals in DRI, should be considered first for recovery. Therefore, the experiments on the effect of smelting conditions on Fe and Cu recovery and quality of the master alloy were carried out systematically.

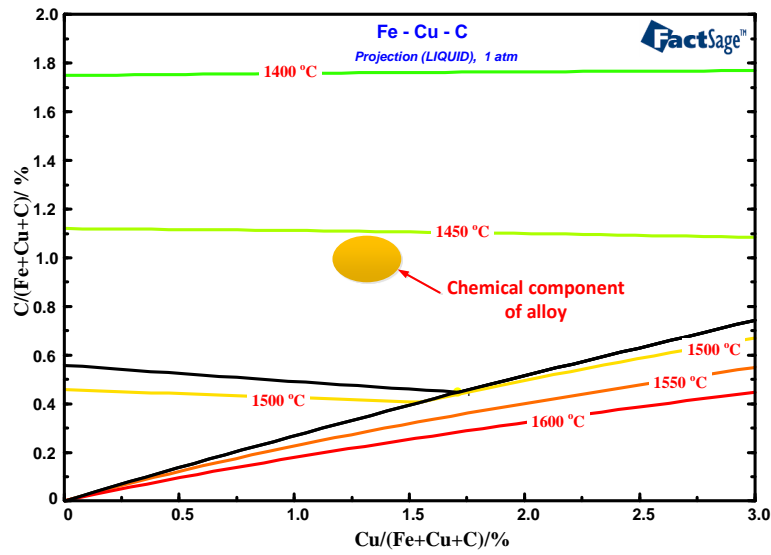


Figure 4. Phase diagram of Fe–Cu–C.

3.2.1. Effect of Smelting Temperature

Undoubtedly, smelting temperature has a significant effect on the smelting process. The effect of the smelting temperature on Fe and Cu recovery and the quality of the master alloy was investigated. The results (Figure 5) show that with an increase in the smelting temperature, the Fe and Cu recovery is elevated and maintained approximately 96%. Additionally, the S content of the master alloy decreased sharply and was maintained at 0.13%. When the smelting temperature was over 1550 °C, all indexes slightly changed.

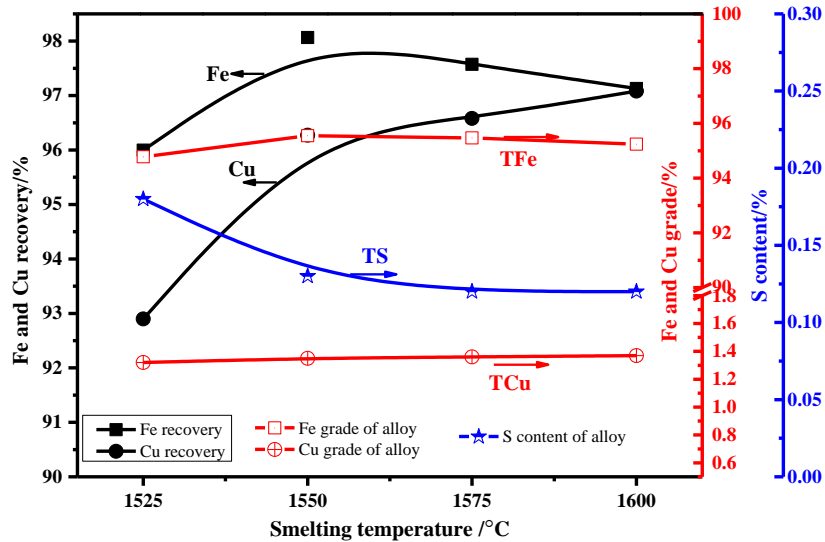


Figure 5. Effect of smelting temperature on Fe and Cu recovery and S removal (Smelting for 30 min with 0.7 binary basicity).

Generally, high temperatures are beneficial for improving the fluidity and decreasing the viscosity of molten slag, thus, resulting in a better settling and separation of the alloy particles. Therefore, the recovery of Fe and Cu increased as the temperature increased. In addition, the desulfurization reaction in the smelting process is an endothermic reaction, and higher temperatures are favourable for the desulfurization in view of the thermodynamics principles. Furthermore, based on dynamics theory, higher temperatures are also capable of promoting the diffusion of S^{2-} and O^{2-} ions from an alloy phase to a slag phase, and ultimately improve the desulfurization efficiency [23].

Therefore, the suitable smelting temperature for the smelting of CBDRI is suggested at 1550 °C, which is in accordance with the thermodynamics analysis.

3.2.2. Effect of Smelting Duration

Smelting duration is believed to have a significant effect on the Fe and Cu recovery and the Fe–Cu master alloy quality. Figure 6 shows the effect of the smelting duration on the Fe and Cu grade and recovery and the removal of S. As the smelting duration increased from 10 min to 40 min, the Fe and Cu recovery increased from 94.4% and 93.8% to 98.2% and 95.8%, respectively. Correspondingly, the S content of the Fe–Cu master alloy presented a decreasing trend from 0.18% to 0.1%. Furthermore, the Fe and Cu grade of the master alloy changed slightly. When the smelting duration was further prolonged, the Fe and Cu recovery and S content were improved insignificantly.

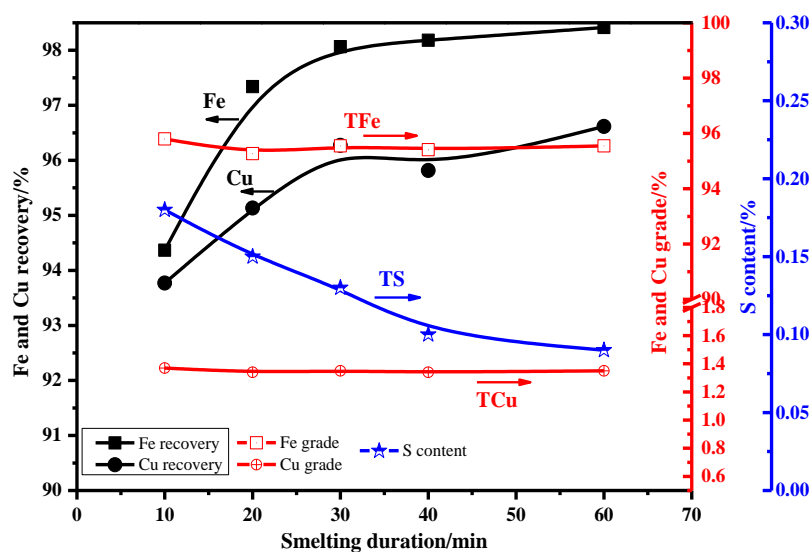


Figure 6. Effect of smelting time on Fe and Cu recovery and S removal (Smelting at 1550 °C with 0.7 basicity).

These results imply that the insufficient smelting time cannot ensure that the desulfurization reaction and the settling of the Fe–Cu master alloy will carry out thoroughly, thus, leading to low metal recovery and poor alloy quality. Therefore, 40 min is appropriate for the simultaneous recovery of Fe and Cu and the removal of S.

3.2.3. Effect of Binary Basicity

The influence of binary basicity on Fe and Cu recovery and the removal of S illustrated in Figure 7 and demonstrates that the binary basicity had a prominent effect on the smelting effect. Fe and Cu recovery first rose and then dropped as the binary basicity increased from 0.3 to 1.5. The recovery of Fe and Cu reached a maximum value of 98.6% and 97.2%, respectively, at 1.0 basicity when the basicity changed from 0.3 to 1.5. While the S content of the Fe–Cu master alloy decreased from 0.150% to 0.039% during the binary basicity test. These results suggest that approximate basicity is in favour of the separation between the Fe–Cu alloy and slag, and the removal of S.

The influence of binary basicity on the smelting process may be due to changes in slag viscosity. The contour map of the change in the viscosity at various temperatures and basicity's is shown in Figure 8. The map illustrates that raising the temperature or approximately increasing the binary basicity is beneficial in improving the slag fluidity. It is worth noting that excessively high or low binary basicity results in a higher viscosity of the molten slag. Limestone can break the silicate and aluminosilicate bonds, and thereby increase the fluidity of the slag [24]. However, when the basicity is over 1.1 (e.g., the addition of limestone is excessive), less liquid phase (as seen in Figure 9) and

more refractory solids, such as Ca_2SiO_4 (as seen in Figure 3), are generated, therefore, resulting in a molten slag with poor fluidity, which is detrimental to the smelting kinetics and phase separation. Ultimately, a basicity over 1.1 leads to low recovery of the Fe and Cu. Moreover, the viscosity of the slag will tend to be at its minimum when the basicity is controlled in a range of 0.9~1.1. Therefore, based on the experimental results, the optimum basicity is recommended at 1.0.

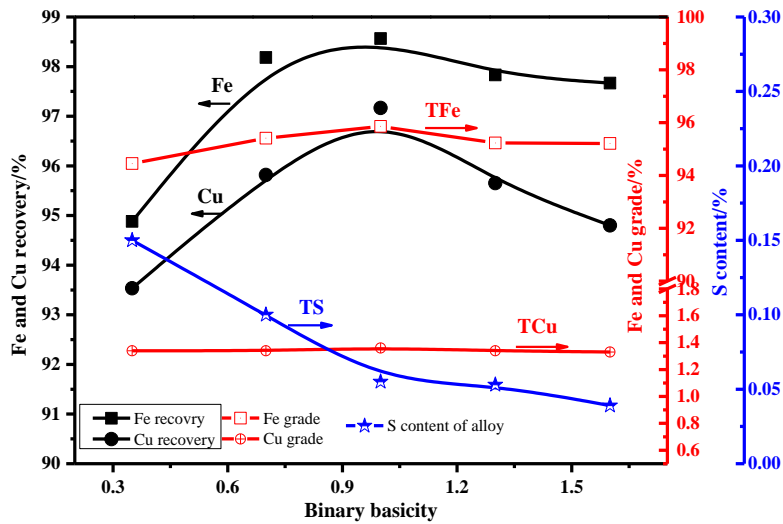


Figure 7. Effect of basicity on Fe and Cu recovery and S removal (Smelting at 1550 °C for 40 min).

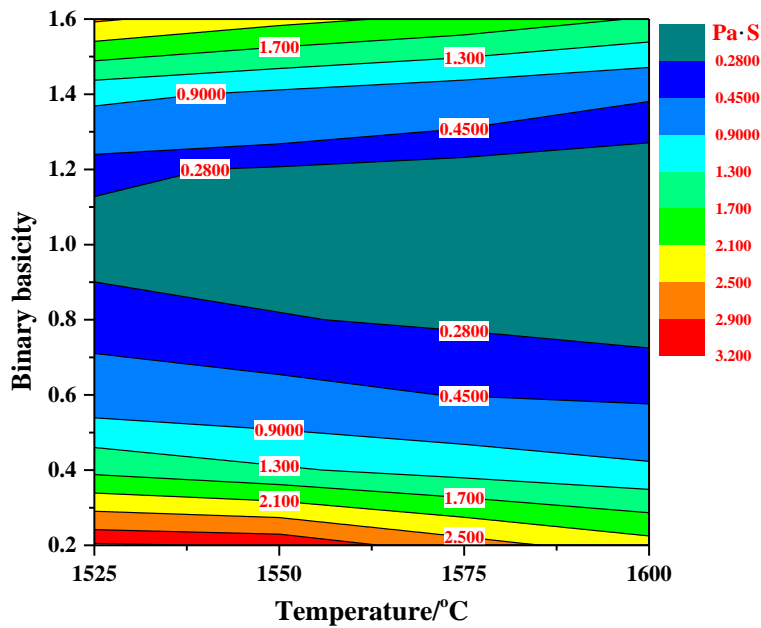


Figure 8. Contour map of viscosity change with various temperatures and basicity.

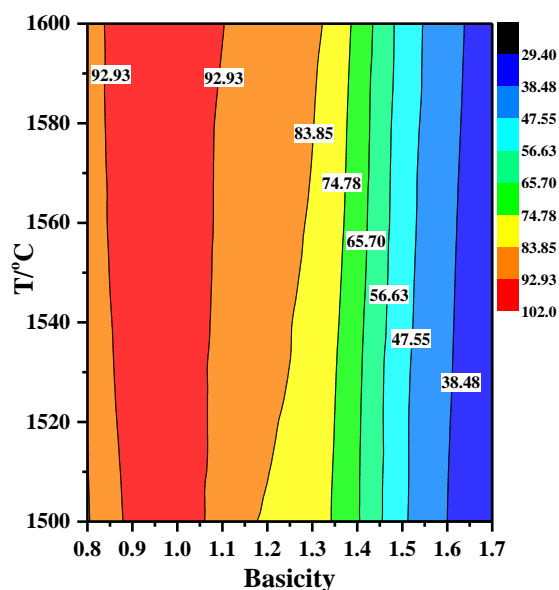


Figure 9. Effect of basicity and temperature on percentage of liquid phase in slag.

3.3. Mechanism of Desulfurization

It is well known that sulfur has adverse effects on the performance of steel products, such as its strength, ductility, and toughness [25]. As noted in the above experimental results, the basicity of the slag plays a significant role in desulfurization during the smelting process. To further reveal the mechanism of desulfurization, the sulfide capacity of the slag was calculated and the desulfurization kinetics were investigated.

3.3.1. Sulfide Capacity (CS) of Slag

The sulfide capacity (CS) and equilibrium distribution ratio of sulfur (LS) are important indicators for measuring the desulfurization capacity of a slag system. In this paper, the optical basicity model was introduced to predict the CS of various slags with different basicity's [23,26]. Optical basicity was calculated by the model shown in Equation (2):

$$\Lambda = \sum_{B=1}^n \chi_B \Lambda_B \quad (2)$$

where Λ is optical basicity, χ_B is mole fraction of oxide cations, which is also defined as the fraction of each cationic charge neutralizing the negative charge.

Hence, the χ_B can be calculated as the following:

$$\chi_B = n_o \chi'_B / \sum n_o \chi'_B \quad (3)$$

where χ'_B is the mole fraction of oxides, n_o is the number of oxygen in each oxide component.

Combining Equation (2) with (3), Young's model was adopted to calculate the sulfide capacity in Equation (4), because it is an easy calculation, has a wide application scope and a high level of accuracy [27,28].

$$\lg CS = -13.913 + 42.84\Lambda - \frac{11710}{T} - 0.02223w(\text{SiO}_2) - 0.02275w(\text{Al}_2\text{O}_3) \quad (4)$$

where CS is the sulfide capacity of slag, Λ is optical basicity; $w(\text{SiO}_2)$ is mass fraction of SiO_2 in slag, $w(\text{Al}_2\text{O}_3)$ is mass fraction of Al_2O_3 in slag.

Based on Equation (4), the sulfide capacity of the various slags with different basicity's can be calculated and the results are shown in Figure 10. The temperature and basicity have a positive effect on the sulfide capacity of the slag. The sulfide capacity increases by increasing the basicity and temperature. This result means that the slag with the higher basicity has a greater ability to hold and remove more sulfide from the metal phase, resulting in an improvement in desulfurization efficiency and lower S content in the Fe–Cu master alloy. The results of the theoretical calculations agree with the experiments shown in Figures 5 and 7.

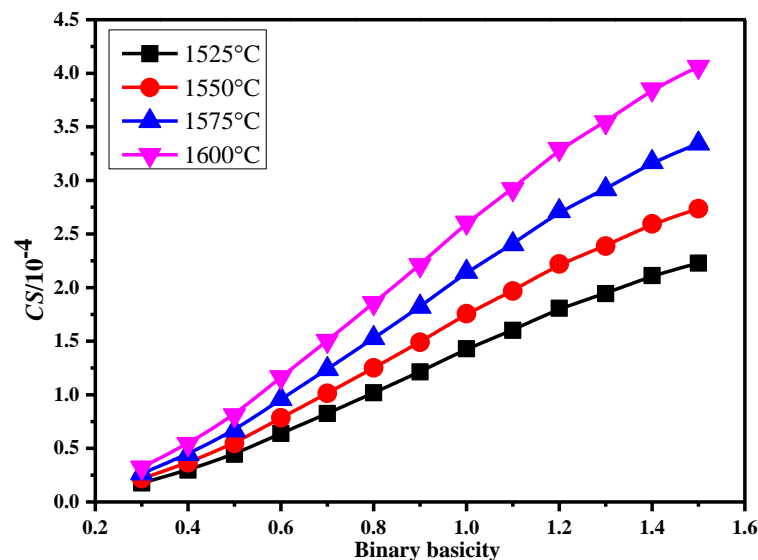


Figure 10. Effect of basicity and temperature on CS of the slag.

3.3.2. Desulfurization Reaction Kinetics of Slag with Different Basicity

As previous work has shown, the desulfurization process consists of five steps: (1) mass transfer of [S] from the metal phase to the interface between the metal and slag; (2) mass transfer of (O^{2-}) from the molten slag to the interface between the metal and slag; (3) an interfacial electrochemical reaction at the interface of the metal and slag; (4) mass transfer of the S^{2-} generated in interfacial chemical reaction from the interface to the molten slag; (5) mass transfer of O^{2-} generated in the interfacial chemical reaction from the interface to the molten metal [28,29].

Compared with the diffusion steps, the rate of the electrochemical interfacial reaction is much faster under a high smelting temperature. In view of that, the overall desulfurization rate is controlled by the mass transfer. Moreover, the diffusion coefficient of S is tens of times higher than that of O, and the diffusion coefficient of sulfur in the metal is about two orders of magnitude larger than that in the slag phase [28–30]. Hence, the control process of the desulfurization reaction is the mass transfer of S in the slag, which was also confirmed by previous work [28,30–32]. Based on this result, the desulfurization rate equation can be expressed as the following:

$$-\frac{d[\%S]}{dt} = \frac{A}{V_m} \cdot K([\%S] - [\%S]^*) \quad (5)$$

where $[\%S]$ is the S content of molten metal, $[\%S]^*$ is the S content of the metal-slag interface, K is the diffusion coefficient, V_m is the volume of molten metal, A is the interface area.

By integrating Equation (5), the following rate formulas could be deduced as follows:

$$\ln \frac{[\%S]_0 - [\%S]_F}{[\%S]_t - [\%S]_F} = k \frac{1}{H} t \quad (6)$$

where $[\%S]_0$ is the S content in the molten metal at the initial stage, $[\%S]_t$ is the S content in the molten metal at a time (t) during the reaction, $[\%S]_F$ is the S content in the molten metal under equilibrium conditions, H is the height of the molten metal, k is the diffusion coefficient, t is the reaction time.

Figure 11 shows the change in sulfur content with time and slag basicity in the alloy samples. By prolonging the reaction time, the S content in the metal decreased. Additionally, increasing the slag basicity can also significantly lower the S content in the metal.

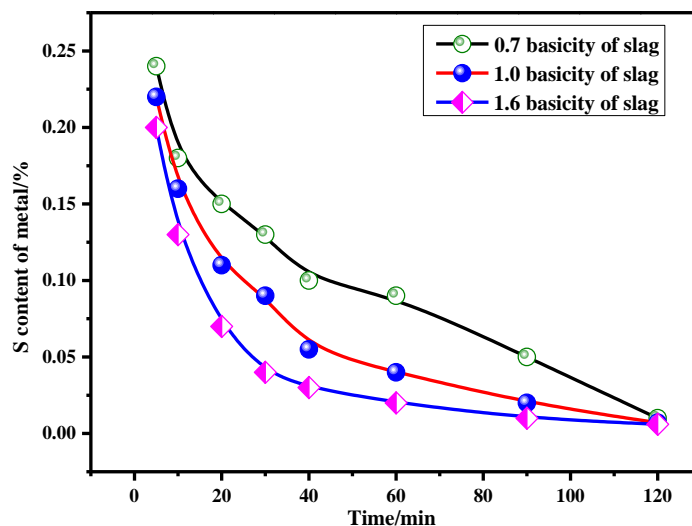


Figure 11. Effects of time and basicity on S content of metal (Smelting temperature 1550 °C).

The plots of $\ln \frac{[\%S]_0 - [\%S]_F}{[\%S]_t - [\%S]_F}$ with the reaction times of for different slag basicity are shown in Figure 12, indicating that the test dates ($\ln \frac{[\%S]_0 - [\%S]_F}{[\%S]_t - [\%S]_F}$) consist well with the theoretical curve in the smelting process at the various basicity's of slag. The standard deviation value of the fitted curves was all over 0.96, which revealed that $\ln \frac{[\%S]_0 - [\%S]_F}{[\%S]_t - [\%S]_F} \sim t$ was a preferable linear relationship. Furthermore, it confirmed that the control process of the total desulfurization reaction was the mass transfer of $[S]$ in the metal phase.

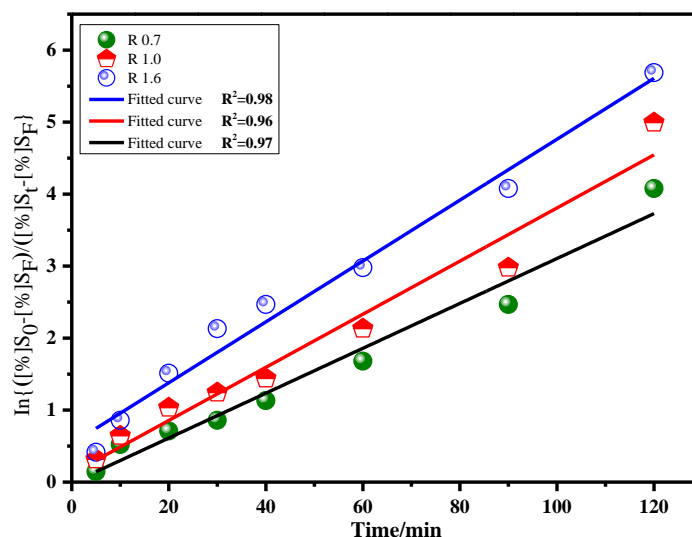


Figure 12. Relation curve between $\ln \frac{[\%S]_0 - [\%S]_F}{[\%S]_t - [\%S]_F}$ and t .

According to the slope of the line for the fitted curves (as seen in Figure 12), the diffusion coefficient can be determined, and the results are shown in Table 3. The diffusion coefficient for desulfurization reaction of 0.7 basicity slag was 0.78×10^{-3} cm/s, whereas increasing the basicity to 1.0 and 1.6,

the diffusion coefficient elevated to 0.92×10^{-3} cm/s and 1.05×10^{-3} cm/s, respectively. These results mean that the slag basicity can promote the mass transfer of S in the slag phase and accelerate the progress of the desulfurization reaction. As a result, the higher basicity allows for better desulfurization efficiency and lower S content of the Fe–Cu alloy.

Table 3. Diffusion coefficient of sulphur in alloy melt (cm/s).

Items	Basicity R		
	0.7	1.0	1.6
Diffusion coefficient	0.78×10^{-3}	0.92×10^{-3}	1.05×10^{-3}

3.4. Characterization of the Fe–Cu Master Alloy

The superior Fe–Cu master alloy can be obtained under the optimum smelting conditions of 1550 °C, 40 min and 1.0 basicity. The chemical composition of the Fe–Cu master alloy is shown in Table 4. The alloy contains 95.9% Fe, 1.4% Cu and some minor impurities. The total content of valuable metals is as high as 97.3%. In addition, the S content of the master alloy decreased to 0.055%. The final product can be used along with scrap steel for the preparation of Cu-bearing steel by electric arc furnace.

Table 4. Chemical compositions of Fe–Cu master alloy (wt %).

Fe	Cu	S	SiO ₂	Al ₂ O ₃	CaO	MgO	Na ₂ O	P	Zn	Pb
95.86	1.36	0.055	0.10	0.32	0.053	0.027	0.005	0.01	0.01	0.009

Figure 13 shows the microstructures of master alloy and chemical compositions under SEM and EDS. These results show that the master alloy is very uniform and pure. Through EDS analysis of a micro zone, the alloy contains 98.6% Fe and 1.4% Cu, and no obvious impurities were found, which further confirms the good performance of this master alloy.

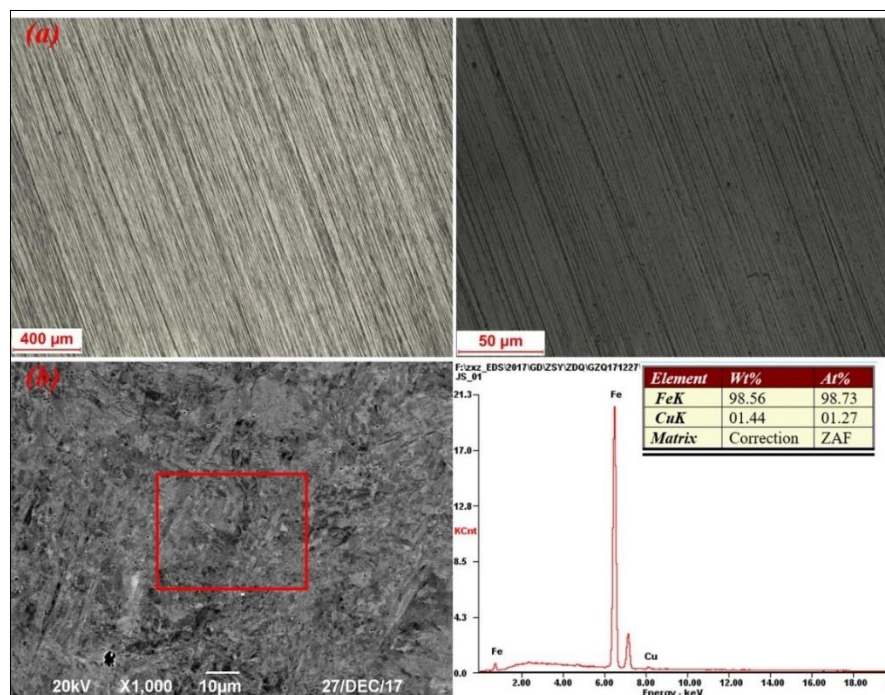


Figure 13. SEM-EDS and microstructure of Fe–Cu alloy.

4. Conclusions

Experimental studies for the smelting process of CBDRI to prepare the Cu-bearing steel master alloy have been carried out in this work, and the mechanism of desulfurization was revealed as well. The following conclusions can be drawn:

(1) A high quality Fe–Cu master alloy, assaying 95.9% Fe, 1.4% Cu and minor impurities, can be obtained from the smelting process under the optimum conditions of 1550 °C, 40 min and 1.0 basicity. The corresponding iron and copper recoveries are 98.6% and 97.2%, respectively. Through the smelting process, the total metal content in the alloy was increased, and the S content was significantly decreased to 0.05%, which is beneficial to the production of clean steel. It also confirms the necessity of further smelting for CBDRI.

(2) Suitable basicity of the molten slag favours an increase in the recovery of Fe and Cu, which results from a rise in the amount of liquid and the improvement in the slag fluidity. In particular, the optimum binary basicity is in the range of 0.9~1.1.

(3) The theoretical calculation results show that the sulfur capacity of the slag elevated with the increasing temperature and basicity, which benefits the desulfurization efficiency. The desulfurization reaction kinetics show that increasing the slag basicity contributes to the diffusion coefficient of the sulfur in the molten slag.

Author Contributions: D.Z., Z.G. and J.P. conceived and designed the experiments; Z.G. and L.P. performed the experiments; Z.G. and L.P. wrote the paper; D.Z. modified the paper.

Funding: This research was funded by National Natural Science Foundation of China (No.51474161) and Innovation-driven Project of Guangxi Zhuang Autonomous Region (No. AA18242003, No. AA148242003).

Acknowledgments: The authors wish to express thanks to the National Natural Science Foundation of China (No. 51474161) for the financial support of this research, and also would like to thank Co-Innovation Center for Clean and Efficient Utilization of Strategic Metal Mineral Resources of Hunan Province, which supplied us the facilities and funds to fulfill the experiments.

Conflicts of Interest: The authors declare no conflict of interest.

References

1. Shi, X.B.; Yan, W.; Xu, D.K.; Yan, M.C.; Yang, C.G.; Shan, Y.Y.; Yang, K. Microbial corrosion resistance of a novel Cu-bearing pipeline steel. *J. Mater. Sci. Technol.* **2018**, *34*, 2480–2491. [[CrossRef](#)]
2. Cao, Z.Q.; Zhao, J.; Yang, K. Cu-bearing stainless steel reduces cytotoxicity and crystals adhesion after ureteral epithelial cells exposing to calcium oxalate monohydrate. *Sci. Rep.* **2018**, *8*. [[CrossRef](#)] [[PubMed](#)]
3. Zhang, X.R.; Zhao, J.L.; Xi, T.; Shahzad, M.B.; Yang, C.G.; Yang, K. Dissolution and repair of passive film on Cu-bearing 304L stainless steels immersed in H₂SO₄ solution. *J. Mater. Sci. Technol.* **2018**, *34*, 2149–2159. [[CrossRef](#)]
4. Morcillo, M.; Díaz, I.; Chico, B.; Cano, H.; Fuente, D. Weathering steels: From empirical development to scientific design. A review. *Corros. Sci.* **2014**, *83*, 6–31. [[CrossRef](#)]
5. Morcillo, M.; Chico, B.; Díaz, I.; Cano, H.; Fuente, D. Atmospheric corrosion data of weathering steels. A review. *Corros. Sci.* **2013**, *77*, 6–24. [[CrossRef](#)]
6. Ma, T.; Yang, G.Y.; Deng, M.L.; Liu, Y.G. Research Status and Prospect of Copper-bearing Steel. *Hot Work. Technol.* **2017**, *46*, 36–39. (In Chinese)
7. Shyi, W.; Powe, K. Effect of alloying elements on the structure and mechanical properties of ultra low carbon bainitic steels. *Mater. Sci.* **1993**, *28*, 5169–5175.
8. Guo, Z.Q.; Pan, J.; Zhu, D.Q.; Zhang, F. Co-reduction of Copper Smelting Slag and Nickel Laterite to Prepare Fe-Ni-Cu Alloy for Weathering Steel. *JOM* **2018**, *70*, 150–154. [[CrossRef](#)]
9. Li, S.W.; Pan, J.; Zhu, D.Q.; Guo, Z.Q.; Xu, J.W.; Chou, J.L. A novel process to upgrade the copper slag by direct reduction-magnetic separation with the addition of Na₂CO₃ and CaO. *Powder Technol.* **2019**, *347*, 159–169. [[CrossRef](#)]
10. Guo, Z.Q.; Zhu, D.Q.; Pan, J.; Yao, W.J.; Xu, W.Q.; Chen, J.A. Effect of Na₂CO₃ Addition on Carbothermic Reduction of Copper Smelting Slag to Prepare Crude Fe-Cu Alloy. *JOM* **2017**, *69*, 1688–1695. [[CrossRef](#)]

11. Gorai, B.; Jana, R.; Premchand, M. Characteristics and utilization of copper slag—a review. *Resour. Conserv. Recycl.* **2003**, *39*, 299–313. [[CrossRef](#)]
12. Subrata, R.; Amlan, D.; Sandeep, R. Flotation of copper sulphide from copper smelter slag using multiple collectors and their mixtures. *Int. J. Miner. Process.* **2015**, *34*, 43–49.
13. Guo, Z.Q.; Pan, J.; Zhu, D.Q.; Zhang, F. Green and efficient utilization of waste ferric-oxide desulfurizer to clean waste copper slag by the smelting reduction-sulfurizing process. *J. Clean. Prod.* **2018**, *199*, 891–899. [[CrossRef](#)]
14. Li, Y.; Perederiy, I.; Papangelakis, V.G. Cleaning of waste smelter slags and recovery of valuable metals by pressure oxidative leaching. *J. Hazard. Mater.* **2008**, *152*, 607–615. [[CrossRef](#)] [[PubMed](#)]
15. Shibayama, A.; Takasaki, Y.; William, T.; Yamatodani, A.; Higuchi, Y.; Sunagawa, S.; Ono, E. Treatment of smelting residue for arsenic removal and recovery of copper using pyro-hydrometallurgical process. *J. Hazard. Mater.* **2010**, *181*, 1016–1023. [[CrossRef](#)] [[PubMed](#)]
16. Perederiy, I.; Papangelakis, V.G.; Buarzaiga, M.; Mihaylov, I. Co-treatment of converter slag and pyrrhotite tailings via high pressure oxidative leaching. *J. Hazard. Mater.* **2011**, *194*, 399–406. [[CrossRef](#)]
17. Antonijevic, M.M.; Dimitrijevic, M.D.; Stevanovic, Z.O.; Serbula, S.M.; Bogdanovic, G.D. Investigation of the possibility of copper recovery from the flotation tailings by acid leaching. *J. Hazard. Mater.* **2008**, *152*, 23–34. [[CrossRef](#)]
18. Zuo, Z.L.; Yu, Q.B.; Xie, H.Q.; Wang, K.; Liu, S.H.; Yang, F.; Qin, Q.; Qi, Z.F. Mechanical and reduction characteristics of cold-pressed copper slag pellets composited within biomass and lignite. *Renew. Energy* **2018**, *125*, 206–224. [[CrossRef](#)]
19. Guo, Z.Q.; Zhu, D.Q.; Pan, J.; Zhang, F. Innovative methodology for comprehensive and harmless utilization of waste copper slag via selective reduction-magnetic separation process. *J. Clean. Prod.* **2018**, *187*, 910–922. [[CrossRef](#)]
20. Chun, T.; Mu, G.; Di, Z.; Long, H.; Ning, C.; Li, D. Recovery of iron from copper slag by carbothermic thermic reduction and magnetic separation in the presence of CaO. *Arch. Metall. Mater.* **2018**, *63*, 299–305.
21. Geng, C.; Wang, H.J.; Hu, W.T.; Li, L.; Shi, C.S. Recovery of iron and copper from copper tailings by coal-based direct reduction and magnetic separation. *J. Iron Steel Res. Int.* **2017**, *24*, 991–997. [[CrossRef](#)]
22. Jiao, R.M.; Xing, P.; Wang, C.Y.; Ma, B.Z.; Chen, Y.Q. Recovery of iron from copper tailings via low-temperature direct reduction and magnetic separation: Process optimization and mineralogical study. *Int. J. Min. Met. Mater.* **2017**, *24*, 974–982. [[CrossRef](#)]
23. Wang, X.H. *Ferrous Metallurgy (Steelmaking Part)*, 1st ed.; Metallurgical Industry Press: Beijing, China, 2007. (In Chinese)
24. Liu, Y.; Lv, X.; Xu, J.; Zhang, S.; Bai, C. Preparation of stainless steel master alloy by direct smelting reduction of Fe–Ni–Cr Sinter at 1600 °C. *Ironmak. Steelmak.* **2016**, *8*, 1–7. [[CrossRef](#)]
25. Yan, Z.; Lv, X.; Pang, Z.; He, W.; Liang, D.; Bai, C. Transition of Blast Furnace Slag from Silicate Based to Aluminate Based: Sulfide Capacity. *Metall. Mater. Trans. B* **2017**, *48*, 2607–2613. [[CrossRef](#)]
26. Guo, H. *Metallurgical Physical Chemistry*, 2nd ed.; China Metallurgical Industry Press: Beijing, China, 2012. (In Chinese)
27. Young, R.W.; Duffy, J.A.; Hassall, G.J. Use of optical basicity concept of determining phosphorus and sulfur slag-metal partitions. *Ironmak. Steelmak.* **1992**, *19*, 201–209.
28. Wang, L.; Wu, S.; Kou, M.; Du, B.; Lu, Y.; Gu, K. Improving the Desulphurization in COREX Process by Adjusting the Hot Metal Chemical Composition. *Metall. Mater. Trans. B* **2018**, *49*, 89–96. [[CrossRef](#)]
29. Wang, X.L. *Ferrous Metallurgy (Ironmaking Part)*, 3rd ed.; China Metallurgical Industry Press: Beijing, China, 2013. (In Chinese)
30. Kang, J.G.; Shin, J.H.; Chung, Y.; Park, J.H. Effect of Slag Chemistry on the Desulfurization Kinetics in Secondary Refining Processes. *Metall. Mater. Trans. B* **2017**, *48*, 2123–2135. [[CrossRef](#)]
31. Peter, J.; Peaslee, K.D.; Robertson, D.G.C.; Thomas, B.G. *Proceedings of the AISTech 2005*; AIST: Warrendale, PA, USA, 2005; pp. 959–967.
32. Robertson, D.G.C.; Staples, B.B. *Process Engineering of Pyrometallurgy*; IMM: London, UK, 1974; pp. 51–59.

